Elastocytosis

Gaetano Napoli* and Alain Goriely†
*Dipartimento di Matematica e Fisica 'E. De Giorgi', Università del Salento, Italy,
†Mathematical Institute, University of Oxford, UK

August 27, 2020

Abstract

Endocytosis and exocytosis are key mechanisms in cellular systems by which a cell deforms its plasma membrane to move substances in or out of the cell. Whereas these cellular processes typically rely on active mechanisms, we study here the problem of achieving encapsulation by a purely physical process. We consider an ideal system in which a rigid particle is put in contact with a spherical deformable body. Depending on the interaction energy between both objects and the mechanical response of the body, partial or total encapsulation may reduce the total energy of the system. In this case, the system would evolve naturally so that the particle will be partially or completely engulfed by the body, a process that we refer to as partial or complete *elastocytosis*. We consider three systems of increasing complexity and we show that elastocytosis is a generic mechanism that can always be achieved in some parameter regimes.

1 Introduction

A key problem for biological cells is to carry material across their membranes. Indeed, while the key function of a membrane is to isolate the cell from the external world, it also needs to interact with its environment by allowing passage through its wall or membrane. A multitude of mechanisms has been developed through evolution to optimize these processes known mostly as endocytosis (inclusion) or exocytosis (exclusion), as coined by de Duve in 1963 [1]. They rely mostly on active transport and the existence of membrane reservoirs [2]. These events are typically mediated by receptor proteins sitting on the membrane and targeting specific molecules with which they interact. A particularly striking example of endocytosis is *phagocytosis* [3, 4]. Phagocyte cells are part of the immune systems and can undergo very large deformations to engulf harmful foreign particles or dead cells that are subsequently removed as shown experimentally [5] and theoretically [6, 7].

While the problem studied here is motivated by these biological mechanisms, the question that we address is whether encapsulation can be achieved through purely physical mechanisms related to the deformation of an elastic body and the interaction energy between particles and cells. We consider an idealized situation in which a spherical (or circular) rigid particle is presented to a deformable spherical (or circular) body. The two bodies interact through direct contact. The interaction energy is taken to be the surface tension when one of the bodies is a liquid droplet or a given adhesion energy when both objects are solids. The rigid particle is initially presented to the deformable body at a single point of contact. The first question is whether a configuration with a contact zone is energetically favorable. If it is the case, the membrane will deform and partially

encapsulate the particle, as shown in Figure 1. The second question is to find the conditions under which the particle will be completely encapsulated. Complete encapsulation is achieved when the membrane folds back and touches itself. By analogy to the biological process of engulfment, we refer to these encapsulations generated by a balance between the tension generated by the adhesion energy and the elastic forces due to the deformation as partial and complete *elastocytosis*.

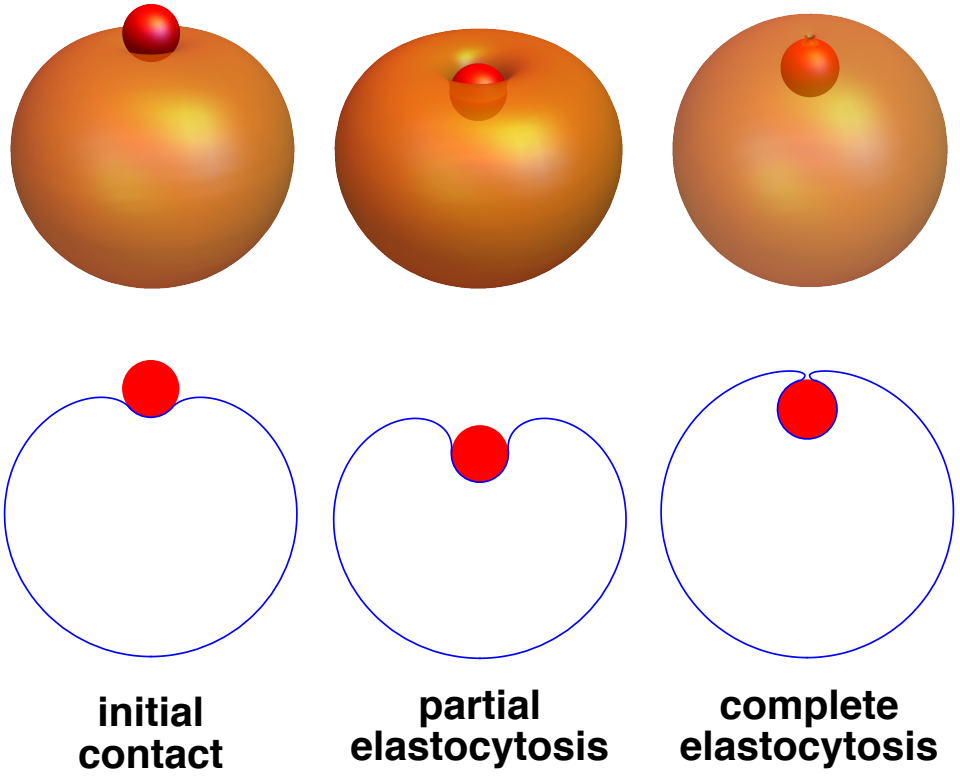

Figure 1: A rigid particle (red) is initially placed into contact with a deformable body. Depending on the system's parameters, it will either (from left to right) remain in contact, be partially engulfed, or be (almost) completely encapsulated.

To elucidate the interplay between physical forces at the membrane level and the deformation and high curvature needed for the engulfment process to take place, we consider three systems of increasing complexity.

First, we look at the problem of a small rigid sphere in contact with a spherical liquid droplet. In this case, the adhesion between the droplet and the particle is entirely determined by the relative surface tensions and the geometry of the system. Therefore, we can use methods from the theory of droplets [8] to classify different behaviors. This process of partial or complete encapsulation of a sphere inside a droplet has been proposed as a possible mechanism for the release of reactive substances in drug delivery [9].

Second, we consider the effect of curvature by looking at the ideal problem of a planar elastic circular rod in contact with a disk. Here, we rely on the theory developed for elastic rods in contact [10] to solve the problem for the shape in terms of two key parameters. Formally, this problem is

equivalent to the plane-strain deformation resulting from the interaction between a solid cylinder and a cylindrical Helfrich fluid membrane that has been considered by different authors [11, 12] and is also reminiscent of the problem of encapsulation in beams [13].

Third, we look at the deformations of an axisymmetric fluid membrane [14, 15, 16] that encapsulates a rigid sphere. This setting is the starting point of many continuous models of cell membranes and directly relevant to the study of giant vesicles [17, 18, 19]. We will show that the three-dimensional problem is markedly different from the planar problem. The interaction between a rigid particle and a soft fluid membrane has been considered in the case of a flat membrane [20], an ellipsoidal nanoparticles [21], impermeable vesicles [22, 23], and soft particles [24, 25]. Other studies, closely related to our analysis, concern the problem of invagination in growing confined lipid membranes [26, 27], the role of particle size [28], and the role of curvature [29] in the wrapping process. Here, we also consider the role played by the saddle-splay term.

2 Adhesion of a liquid droplet with a rigid sphere

When a liquid droplet is put in contact with a solid sphere, three distinct wetting configurations may occur: non-wetting, partial wetting, or complete wetting. These configurations can be predicted based on the different surface tensions involved in the system.

2.1 Model

We consider a droplet of fluid with internal pressure p and surface tension $\gamma_{\mathrm{f}} > 0$. We present to this droplet a rigid sphere of radius r and assume that the difference of the liquid-solid surface tension, γ_{c}, is such that $\gamma_{\mathrm{c}} < \gamma_{\mathrm{f}}$, as shown in Figure 2. For completeness, we briefly recall the basic principles of surface tension theory for droplets (see e.g. [30]). In order to obtain the equilibrium equations, we balance the internal energy W of the system with the work L done by the external actions through the variational principle

$$\delta W = \delta L. \tag{1}$$

Here, the internal energy of the droplet consists of two terms representing the energy of the free interface W_{free} and the energy of contact W_{contact}:

$$W = W_{\mathrm{free}} + W_{\mathrm{contact}}, \qquad W_{\mathrm{free}} = \int_{\Sigma_{\mathrm{f}}} \gamma_{\mathrm{f}} \, \mathrm{d}A, \quad W_{\mathrm{contact}} = \int_{\Sigma_{\mathrm{c}}} \gamma_{\mathrm{c}} \, \mathrm{d}A, \tag{2}$$

where Σ_{f} is the free interface and Σ_{c} the contact surface.

To compute the first variation of the free energy, we assume that Σ_{f} undergoes an infinitesimal virtual deformation $\mathbf{r}' = \mathbf{r} + \epsilon \mathbf{u}$, where ϵ is a small positive parameter, and we use the transport theorem to compute the first variation

$$\delta W_{\mathrm{free}} = \int_{\Sigma_{\mathrm{f}}} \gamma_{\mathrm{f}} \, \mathrm{div}_{\mathrm{s}} \mathbf{u} \, \mathrm{d}A, \tag{3}$$

where $\mathrm{div}_{\mathrm{s}}$ denotes the surface divergence. Using the divergence theorem, (3) can be recast as

$$\delta W_{\mathrm{free}} = \int_{\partial \Sigma_{\mathrm{f}}} \gamma_{\mathrm{f}} (\mathbf{P}\mathbf{k}_{\mathrm{f}}) \cdot \mathbf{u} \, \mathrm{d}l + 2 \int_{\Sigma_{\mathrm{f}}} \gamma_{\mathrm{f}} H \boldsymbol{\nu} \cdot \mathbf{u} \, \mathrm{d}A, \tag{4}$$

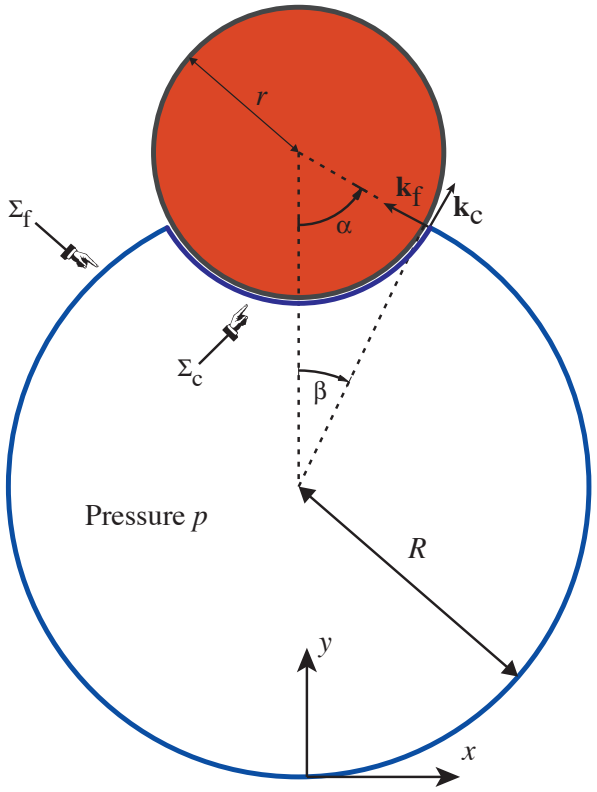

Figure 2: Schematic representation of the equilibrium configuration.

where $\boldsymbol{\nu}$ is the unit outward normal vector to Σ_f, $\mathbf{P}$ is the projection onto the tangent plane, $\mathbf{k}_f$ is the outward normal to the boundary in the tangent plane and H is the mean curvature. Note that by choosing the plus in front of the second term in the right-hand side of (4), we adopt the convention that the mean curvature of a sphere of radius R is equal to $1/R$. The quantity $\boldsymbol{\sigma}_f = \gamma_f \mathbf{P}$ can be interpreted as the tangential stress tensor. In the contact region, the only virtual displacements $\tilde{\mathbf{u}}$ are tangent to rigid surface. Consequently, we have

$$\int_{\partial\Sigma_f} \gamma_f(\mathbf{P}\mathbf{k}_f) \cdot \mathbf{u} \, \mathrm{d}l = \int_{\partial\Sigma_c} \gamma_c(\mathbf{P}\mathbf{k}_c) \cdot \tilde{\mathbf{u}} \, \mathrm{d}l, \tag{5}$$

where $\mathbf{k}_c$ is the outward normal to the boundary of the contact region.

The virtual work done by the internal pressure is

$$\delta L = \int_{\Sigma_f} p\boldsymbol{\nu} \cdot \mathbf{u} \, \mathrm{d}A. \tag{6}$$

The variational principle (1) leads to the Young-Laplace law for the free part of the interface

$$2\gamma_f H = p, \tag{7}$$

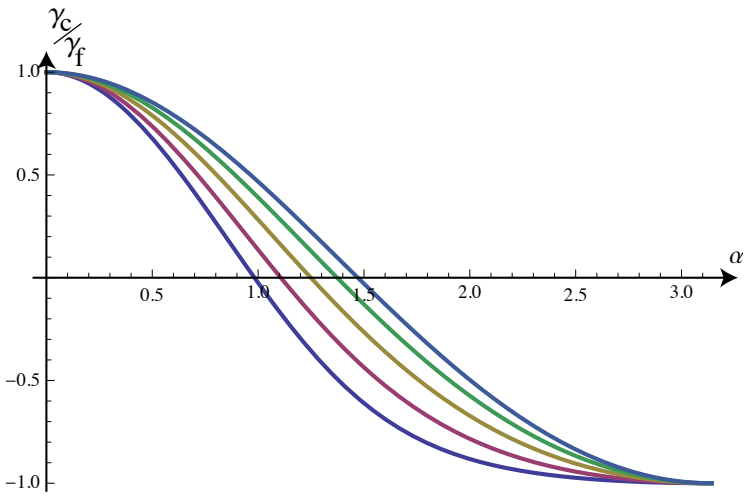

Figure 3: Isobaric wetting. γ_f/γ_c versus the wetting angle α, for $\mu = 1.5, 2, 3, 5, 10$.

and the boundary condition

$$\gamma_f \mathbf{k}_f \cdot \mathbf{k}_c = -\gamma_c. \tag{8}$$

2.2 Analysis

2.2.1 Isobaric wetting

From (7), it follows that the free interface is a portion of a sphere of radius

$$R = \frac{2\gamma_f}{p}. \tag{9}$$

Thus, in a process where p and γ_f are fixed, while the adhesion strength γ_c changes, the radius of the liquid droplet remains constant. Using the angles α and β defined in Figure 2, (8) becomes

$$\cos(\alpha - \beta) = \frac{\gamma_c}{\gamma_f}, \tag{10}$$

with the constraint

$$r \sin\alpha = R \sin\beta. \tag{11}$$

By solving the last two equations, we obtain

$$\frac{\gamma_c}{\gamma_f} = \mu^{-1}(-\sin^2\alpha + \cos\alpha\sqrt{\mu^2 - \sin^2\alpha}), \tag{12}$$

where $\mu = R/r$. Therefore, we conclude that (see Figure 3) for any μ: (i) adhesion ($\alpha > 0$) is possible if $\gamma_c < \gamma_f$; (ii) γ_c/γ_f is a strictly decreasing function of α; (iii) complete encapsulation ($\alpha = \pi$) only occurs when $\gamma_c = -\gamma_f$.

In this setting, the interplay between the internal pressure and the surface tension γ_f fixes the radius of the droplet independently of the adhesion strength γ_c. Thus, by decreasing γ_f the area of the contact region increases as the wetting angle increases, without a change in the droplet radius.

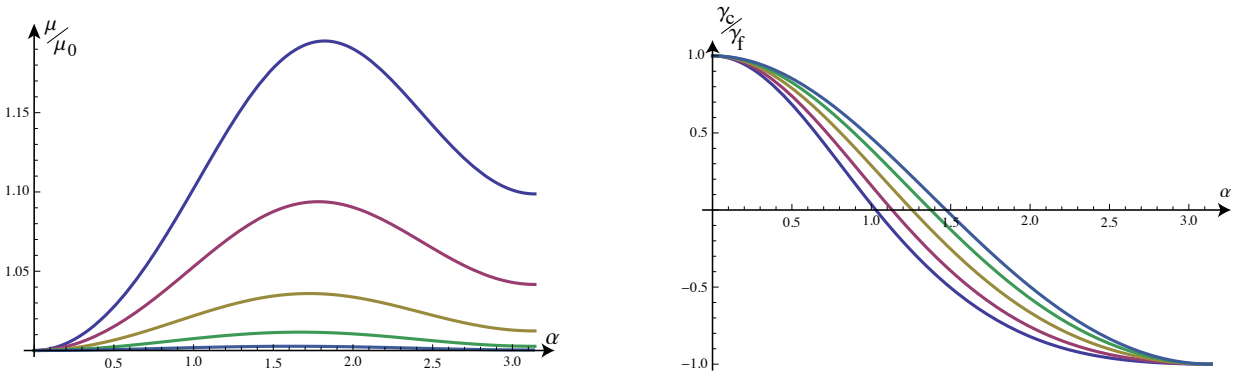

Figure 4: Isochoric wetting. Droplet radius dilatation μ/μ_0 (left) and relative energy adhesion γ_c/γ_f (right) versus the wetting angle α, for $\mu_0 = 1.5, 2, 3, 5, 10$.

2.2.2 Isochoric wetting

In the previous section we analyzed adhesion at constant pressure p but varying volume. Next, we consider the case where the enclosed volume V remains constant. Equations (7) and (8) are still valid, provided that p is now the Lagrange multiplier associated with the volume conservation constraint. From the Young-Laplace law (7) we obtain the pressure $p = 2\gamma_f/R$, where R has to satisfy the volume constraint

$$\frac{4}{3}\pi R^3 - \frac{4}{3}\pi R^3(2+\cos\beta)\sin^4\frac{\beta}{2} - \frac{4}{3}\pi r^3(2+\cos\alpha)\sin^4\frac{\alpha}{2} = V_0, \tag{13}$$

which can be recast in the non-dimensional form

$$\mu^3\left[1-(2+\cos\beta)\sin^4\frac{\beta}{2}\right] - (2+\cos\alpha)\sin^4\frac{\alpha}{2} = \mu_0^3, \tag{14}$$

where $\mu = R/r$ and $\mu_0 = R_0/r$, with R_0 the initial radius of the droplet. The angles α and β have to satisfy Equations (10) and (11). Figure 4 sketches the radius dilation μ/μ_0 as a function of the wetting angle. For large values of μ_0, we obtain the approximate expression

$$\frac{\mu}{\mu_0} \approx 1 + \frac{\sin^2\alpha}{4\mu_0^2} + \frac{2+\cos\alpha}{3\mu_0^3}\sin^4\frac{\alpha}{2}. \tag{15}$$

As in the isobaric case, the area of the contact region increases as the ratio γ_c/γ_f decreases (Figure 4 right).

3 Adhesion of a Euler elastica with a hard disk

Next, we study the equilibrium configurations of an inextensible and unshearable elastic rod of fixed length, closed into a planar ring of radius R, in contact with an adhesive rigid disk of radius r, $(r < R)$, as depicted in Figure 5. We define *elastocytosis* as the elastic equivalent to either endocytosis or exocytosis. During endocytosis, a disk is initially located outside the ring and is partially or completely engulfed due to the fact that a contact zone with adhesion lowers the total energy of the system. Similarly, during exocytosis, the disk is inside the loop and is wrapped due to adhesion.

3.1 Energetic considerations

The elastic energy (density) of a rod shaped as an elastic circular ring of radius R is

$$W_{\text{circ}} = k\pi R\left(\frac{1}{R} - \zeta_0\right)^2, \tag{16}$$

where k is the bending stiffness, while ζ_0 denotes the (signed) intrinsic curvature of the rod (if $\zeta_0 < 0$, the unloaded ring has been inverted and cutting a small part of it would result in an inversion of curvature). In the ideal case of complete elastocytosis, a new circular elastic ring of radius $R - r$ is formed, while the disk is completely coated by the elastic loop to form an *elastosome*. The energy corresponding to these final configurations are

$$W_{\pm} = k\pi(R-r)\left(\frac{1}{R-r} - \zeta_0\right)^2 + k\pi r\left(\frac{1}{r} \pm \zeta_0\right)^2 - 2\pi r\Delta\gamma, \tag{17}$$

where $(+)$ refers to endocytosis and $(-)$ to exocytosis, and $\Delta\gamma > 0$ is the ring-disk adhesion energy density (energy per unit length). If we assume that these configurations are selected through energy minimization, we see that the sign of the spontaneous curvature selects which of the two phases is energetically favored. In fact, $\Delta W = W_+ - W_- = 4\pi k\zeta_0$ and therefore exocytosis is a minimum energy state when $\zeta_0 > 0$, while endocytosis is favored for $\zeta_0 < 0$. Intuitively, if $\zeta_0 > 0$, the ring is initially in a low energy state and the creation of two rings with the same curvature (exocytosis) is preferable to the creation of a large ring of the same curvature and a small one of inverted curvature (endocytosis).

Furthermore, if we compare Equation (17) with (16), we obtain the two critical values

$$(\Delta\gamma)^{\pm} = k\frac{R^2 - r(R-r)(1 \pm 2\zeta_0 R)}{2r^2 R(R-r)}. \tag{18}$$

For adhesion values larger than $(\Delta\gamma)^{\pm}$, the splitting of the initial rings into a smaller ring and an elastosome becomes energetically favorable:

However, as the parameters in the system are varied through this bifurcation, we have no information about how this transition takes place. This information is contained in the intermediary phase where the disk partially adheres to the flexible loop, which we consider next.

3.2 Partial wrapping

Let s denote the arclength measured from the bottom of the circle (Figure 5). A point $p(s)$ on the ring can be parametrized by its Cartesian coordinates $\mathbf{r}(s) = [x(s), y(s)]$ that obey

$$x' = \cos\psi, \quad y' = \sin\psi, \tag{19}$$

where $\psi(s)$ is the angle between the tangent at p and the x-axis.

We consider an inextensible and unshearable closed elastic rod of length $L = 2\pi R$ and restrict our attention to symmetric equilibrium shapes with respect to the y axis. The bending energy functional is then

$$W_{\text{b}}[\psi] = k\int_0^{\bar{s}} (\psi' - \zeta_0)^2 \mathrm{d}s + k\int_{\bar{s}}^{L/2}\left(\frac{1}{r} \pm \zeta_0\right)^2 \mathrm{d}s, \tag{20}$$

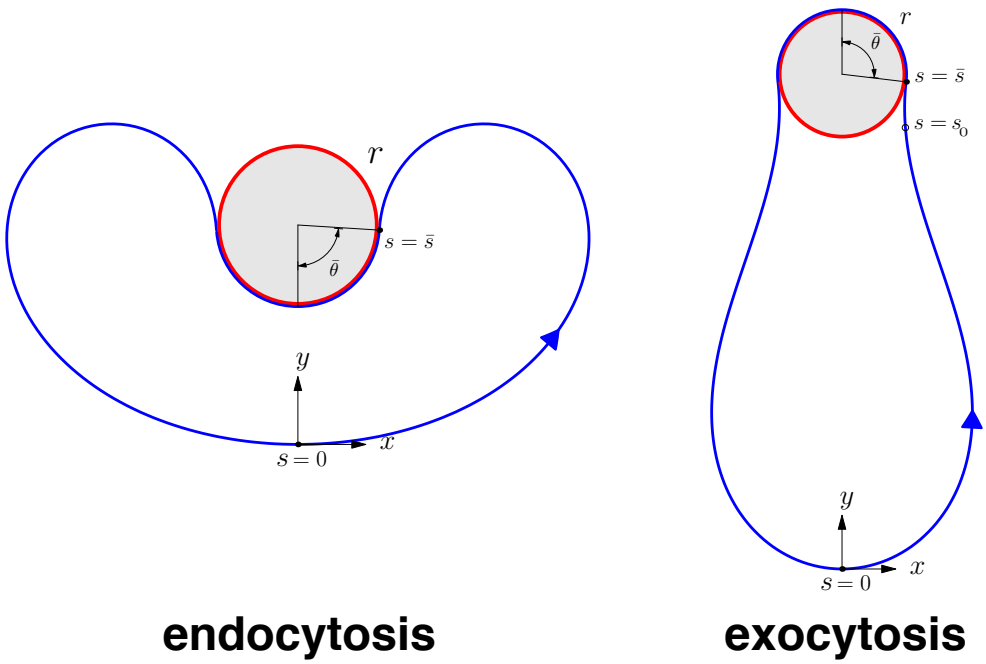

Figure 5: Schematic representation of the equilibrium configuration: endocytosis (left) and exocytosis (right).

where $\bar{s}$ denotes the arclength of the first contact point, and, as before, the plus sign applies in the case of endocytosis (minus for exocytosis). In addition, at the points where the rod is in contact with the rigid disk, there is an adhesion potential of the form

$$W_{\mathrm{a}}[\psi] = -2\Delta\gamma \int_{\bar{s}}^{L/2} \mathrm{d}s. \tag{21}$$

In order to enforce the inextensibility constraint, the following energy terms are added to the energy functional

$$W_{\mathrm{c}}[\psi] = 2n_x \int_0^{\bar{s}} (\cos\psi - x')\mathrm{d}s + 2n_y \int_0^{\bar{s}} (\sin\psi - y')\mathrm{d}s, \tag{22}$$

where n_x and n_y are the unknown Lagrange multipliers associated with the constraint. Physically, they are interpreted as the horizontal and vertical components of the internal force.

The equilibrium shapes are stationary points of the total functional

$$W[\psi] = W_{\mathrm{a}}[\psi] + W_{\mathrm{b}}[\psi] + W_{\mathrm{c}}[\psi]. \tag{23}$$

The corresponding Euler-Lagrange equations associated with W yields

$$k\psi'' + n_x \sin\psi - n_y \cos\psi = 0, \tag{24}$$

and we recover the classical balance of torque for planar rods (see e.g. [31, p. 122]). Without loss of generality, we assume that the rigid disk is presented at the top of the membrane and we fix the

origin of s at the bottom, so that at $s = 0$ we have (Figure 5)

$$x(0) = 0, \qquad y(0) = 0, \qquad \psi(0) = 0. \tag{25}$$

At the contact point $s = \bar{s}$, we define the angle $\bar{\theta}$ to be the angle such that

$$\bar{x} := x(\bar{s}) = r \sin \bar{\theta}. \tag{26}$$

Hence, we define the *wrapping angle*

$$\bar{\theta} = r^{-1}(\pi R - \bar{s}) \tag{27}$$

to be half of the angle subtended by the contact region. This angle will be different for endocytosis or exocytosis (see Figure 5). Explicitly, we have

$$\bar{\psi}_{\pm} := \psi(\bar{s}) = \pi \pm \bar{\theta}, \qquad ((+) \text{ endocytosis, (-) exocytosis}). \tag{28}$$

The fact that the contact point $\bar{s}$ is unknown implies that the minimization process provides a further boundary condition, namely *the transversality condition* [32, 33, 26]

$$\psi'(\bar{s}) = -\left(\pm\frac{1}{r} - \frac{\sqrt{2}}{\ell_{\text{ec}}}\right), \qquad ((+) \text{ endocytosis, (-) exocytosis}), \tag{29}$$

where $\ell_{\text{ec}} := \sqrt{k/\Delta\gamma}$ is the elasto-capillary length, which is the characteristic length scale that quantifies the relative importance of surface forces with respect to elastic rigidity [34]. We note that even though ζ_0 does not enter the equilibrium equations, it plays a crucial role in the total energy.

3.3 Analysis

In the absence of external loads and for symmetric shapes, Equation (24) with $n_y = 0$ is formally equivalent to the pendulum equation through the classic Kirchhoff analogy [35]. Hence, it admits the first integral

$$\frac{(\psi')^2}{2} - h\cos\psi = c, \tag{30}$$

where $h := n_x/k$. The constant c can be obtained by evaluating (30) at $s = \bar{s}$, with the aid of (28) and (29) to give

$$c = \frac{1}{2}\left(-\frac{1}{r} + \frac{\sqrt{2}}{\ell_{ec}}\right)^2 - h\cos\bar{\psi}. \tag{31}$$

3.3.1 Endocytosis

By observing that $\psi(s)$ is a strictly increasing function in $[0, \bar{s}]$, (30) can be integrated by separation of variables to yield

$$\bar{s} = \int_0^{\bar{\psi}} \frac{\mathrm{d}\psi}{\sqrt{2(c + h\cos\psi)}}, \tag{32}$$

whence

$$\bar{s} = \mathrm{F}(q_*)\sqrt{\frac{2}{(c+h)(c+h\cos\bar{\psi})}}, \tag{33}$$

where $\mathrm{F}(\cdot)$ denotes the incomplete elliptic integral of the first kind [36] with

$$q_* := \left[\frac{\bar{\psi}}{2}, \frac{2h}{c+h}\right].$$

Furthermore, Equation $(19)_1$ equipped with the boundary conditions $(25)_1$ and (26) leads to

$$\bar{x} = \int_0^{\bar{\psi}} \frac{\cos\psi \mathrm{d}\psi}{\sqrt{2(c+h\cos\psi)}}, \tag{34}$$

that yields

$$\bar{x} = -\frac{c}{h}\bar{s} + \mathrm{E}(q_*)\frac{\sqrt{2}}{h}\sqrt{c+h}, \tag{35}$$

where $\mathrm{E}(\cdot)$ denotes the incomplete elliptic integral of the second kind [36].

Substitution of (26) and (28) into (31), (33) and (35) leads to

$$c = \frac{1}{2}\left(-\frac{1}{r} + \frac{\sqrt{2}}{\ell_{ec}}\right)^2 + h\cos\bar{\theta}, \tag{36a}$$

$$\bar{s} = \mathrm{F}(q_*)\sqrt{\frac{2}{(c+h)(c-h\cos\bar{\theta})}}, \tag{36b}$$

$$r\sin\bar{\theta} = -\frac{c}{h}\bar{s} + \mathrm{E}(q_*)\frac{\sqrt{2}}{h}\sqrt{c+h}. \tag{36c}$$

These equations, together with Equation (27), can be solved numerically to obtain $\bar{s}$, h, c and $\bar{\theta}$ as functions of all the parameters: ℓ_{ec}, r, and R.

3.3.2 Exocytosis

In the exocytosis case, (see Figure 5), the equilibrium solution $\psi(s)$ increases for $s \in (0, s_0)$, while it decreases for $s \in (s_0, \bar{s})$. We denote $\psi_0 = \psi(s_0) \in [0, \pi]$ to be the maximum value of $\psi(s)$ in the interval $(0, \bar{s})$. Since $\psi'(s_0) = 0$, (30) gives $c = -h\cos\psi_0$. Thus, by integrating (30) by separation of variables over the two intervals where $\psi(s)$ is monotonic, we obtain

$$\bar{s} = \frac{1}{\sqrt{2h}}\int_0^{\psi_0} \frac{\mathrm{d}\psi}{\sqrt{\cos\psi - \cos\psi_0}} - \frac{1}{\sqrt{2h}}\int_{\psi_0}^{\bar{\psi}} \frac{\mathrm{d}\psi}{\sqrt{\cos\psi - \cos\psi_0}}, \tag{37}$$

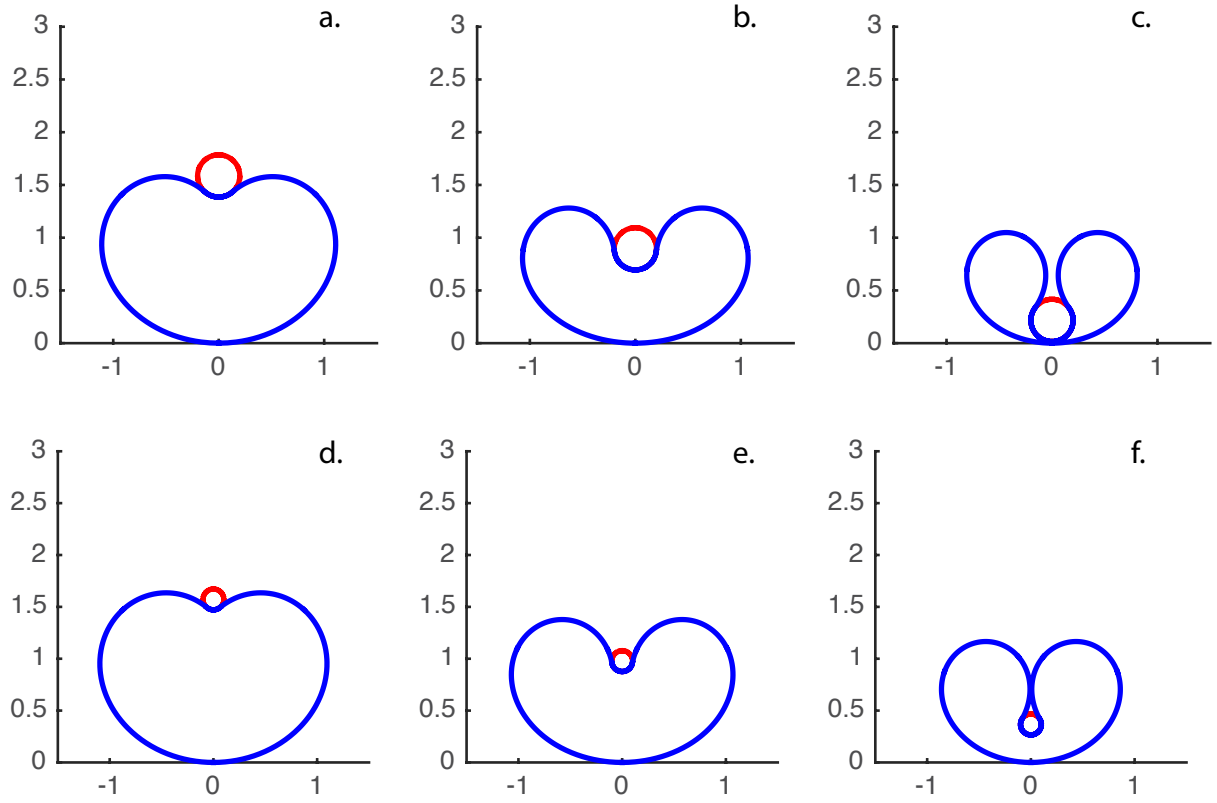

Figure 6: Planar endocytosis equilibrium shapes for $\mu = 5$ (top) ($\eta = 0.94$, $\bar{\theta} = 41°$ (left), $\eta = 0.97$, $\bar{\theta} = 83°$ (center), $\eta = 0.93$, $\bar{\theta} = 125°$ (right)) and $\mu = 10$ (bottom) ($\eta = 0.82$, $\bar{\theta} = 39°$ (left), $\eta = 0.83$, $\bar{\theta} = 72°$ (center), $\eta = 0.81$, $\bar{\theta} = 119°$ (right)).

whence

$$\bar{s} = \frac{2\mathrm{F}(q_0) - \mathrm{F}(\bar{q})}{\sqrt{h}\sin\frac{\psi_0}{2}}, \tag{38}$$

where

$$q_0 := \left[\frac{\psi_0}{2}, \csc^2\frac{\psi_0}{2}\right], \qquad \bar{q} := \left[\frac{\bar{\psi}}{2}, \csc^2\frac{\psi_0}{2}\right]. \tag{39}$$

Similarly, we integrate Equation $(19)_1$ with the boundary conditions $(25)_1$ and (26):

$$\bar{x} = \bar{s}\cos\psi_0 + \frac{2}{\sqrt{h}}\left(2\mathrm{E}(q_0) - \mathrm{E}(\bar{q})\right)\sin\frac{\psi_0}{2}. \tag{40}$$

3.4 Discussion

The model depends on three dimensionless parameters

$$\mu := \frac{R}{r}, \quad \eta := \frac{r}{\ell_{ec}}, \quad \varsigma_0 := \zeta_0 R, \tag{41}$$

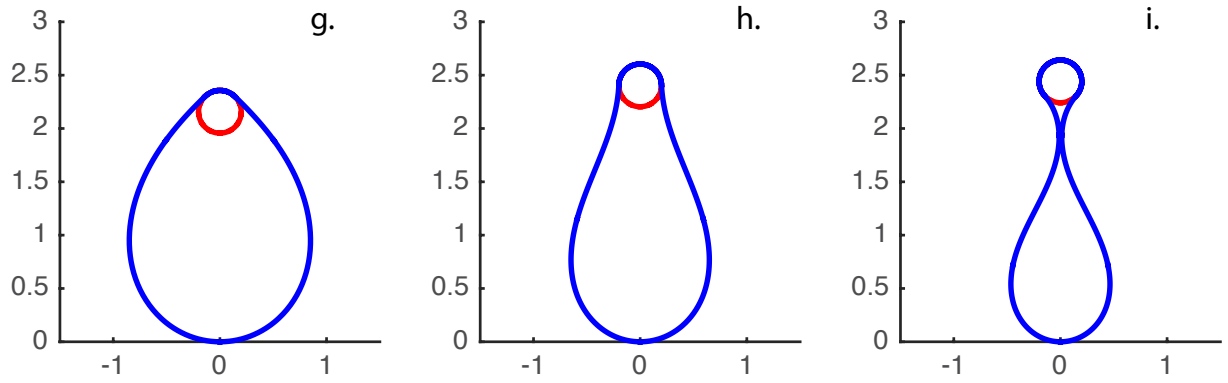

Figure 7: Planar exocytosis equilibrium shapes for $\mu = 5$ ($\eta = 0.67$, $\bar{\theta} = 44°$ (left), $\eta = 0.83$, $\bar{\theta} = 88°$ (center), $\eta = 1.0$ $\bar{\theta} = 132°$ (right)).

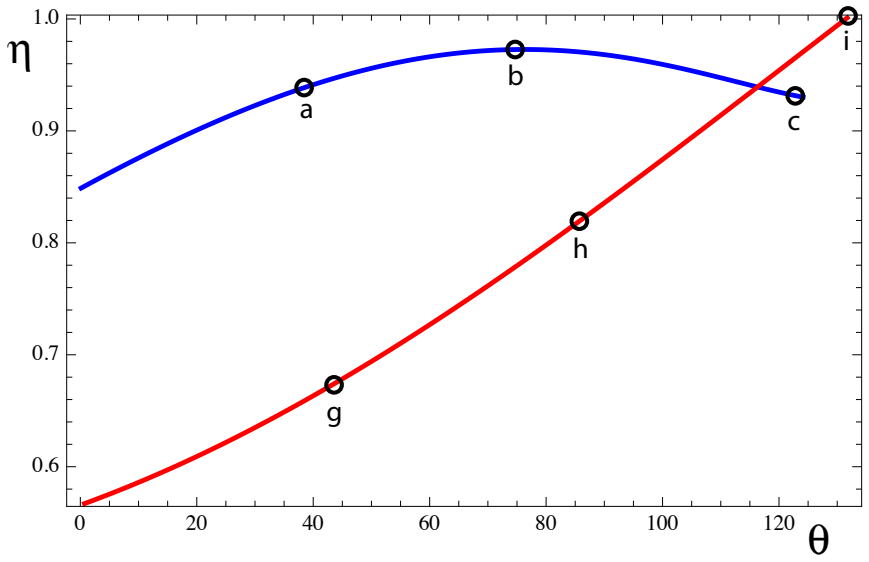

Figure 8: Gluing number η as a function of the wrapping angle $\bar{\theta}$ for endocytosis (blue) and exocytosis (red). The circles correspond to the shapes given in the two previous figures.

which represent, respectively, the ratio between the radii, the gluing number, and the reduced intrinsic curvature. The gluing number, η, is a ratio of the two characteristic physical length scales: the disc curvature (associated with bending) and the elasto-capillary length. At ℓ_{ec} constant, the ring is more likely to adhere on an almost flat surface (small curvature or large r) than on a curved surface (small r). Similarly, for a fixed disc radius, the ability of the ring to adhere increases with the adhesion strength (small ℓ_{ec}) and decreases with the elastic stiffness (large ℓ_{ec}). The reduced intrinsic curvature, μ, is the ratio of the two geometric lengths of the elastica: the radius of the undeformed ring R and the spontaneous curvature radius $1/\zeta_0$. The latter is the natural radius of a small piece of the ring in the absence of stress. Any deviation away from this radius has an energy cost given by (16). In particular, for $\varsigma_0 = 1$, the energy (16) attains it absolute minimum. For elastocytosis, the sign of ς_0 is expected to play an important role since surfaces with curvatures of the same sign have a greater tendency to stick, while surfaces with opposite curvatures tend to separate.

Figures 6 and 7 sketch equilibrium shapes obtained by varying the wrapping angle at fixed μ. During endocytosis small inclusions can self-encapsulate (Figure 6 right-bottom), while for larger ones the bottom self-contact occurs before encapsulation (Figure 6 right-top). During exocytosis the disk can be encapsulated for a sufficiently large gluing number (Figure 7 right).

We see in Figure 8 that wrapping increases with the gluing number during exocytosis (red line) but not during endocytosis (blue line). The value of η corresponding to the circular solution with a single contact point can be computed by observing that $\bar{s} = \pi R$ and $\bar{\psi} = \pi$. Thus, from (30), we deduce that $h = 0$ and, hence, $c = 1/(2R^2)$. This observation, together with (31), leads to the *activation thresholds*

$$\eta^{\pm}_{\text{act}} = \frac{1 \pm \mu^{-1}}{\sqrt{2}}, \qquad ((+) \text{ endocytosis, (-) exocytosis}). \tag{42}$$

Beyond these thresholds, partial wrapping becomes energetically favored compared to the no-contact solution. We note that exocytosis is triggered at a lower threshold than that of endocytosis. Physically, this difference is due to the fact that during exocytosis the curvatures of the surfaces in contact match, while during endocytosis they have opposite signs. Both curves of Figure 8 stop at the point of self-intersection.

To understand the energy landscape, we introduce the dimensionless energy $w = WR/k$, with which Equations (16) and (17) now read

$$w_{\text{circ}} = \pi(1 - \varsigma_0)^2, \tag{43a}$$

$$w_{\text{endo}} = \pi \left(\frac{\mu^2}{\mu - 1} - 2\eta^2\mu + {\varsigma_0}^2 \right) + 4\pi\varsigma_0, \tag{43b}$$

$$w_{\text{exo}} = \pi \left(\frac{\mu^2}{\mu - 1} - 2\eta^2\mu + {\varsigma_0}^2 \right), \tag{43c}$$

while (18) yields the dimensionless thresholds

$$\eta^{\pm} = \sqrt{\frac{1 + \mu^2 - \mu \pm 2\varsigma_0(\mu - 1)}{2\mu(\mu - 1)}}, \qquad ((+) \text{ endocytosis, (-) exocytosis}). \tag{44}$$

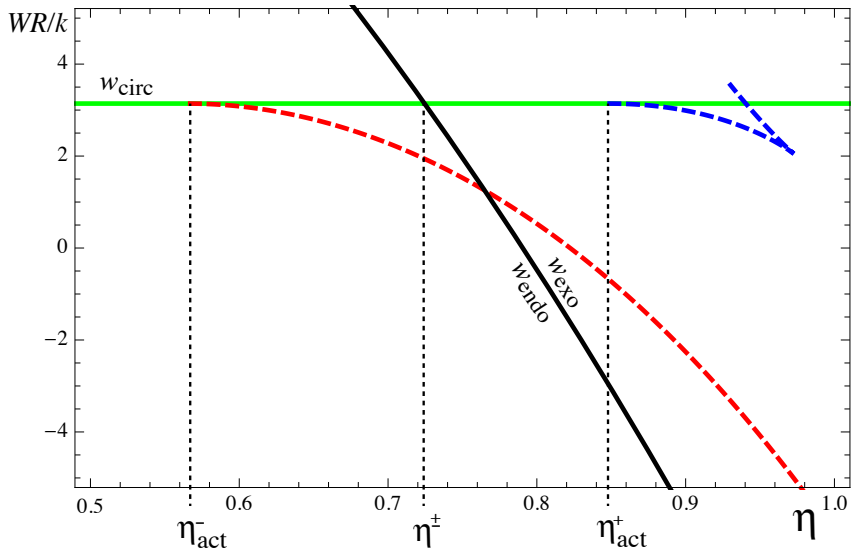

Figure 9: Energy landscape for $\mu = 5$ and $\varsigma_0 = 0$. The green line represents the no-contact solution, while the solid black line corresponds to complete endo/exocytosis. The dashed curves are the energy of partial endocytosis (blue) and partial exocytosis (red).

Figure 9 gives an example of the energy landscape. The partial contact branches, represented by the dashed lines, have been obtained numerically. The green line represents $w_{\rm circ}$, while the solid black line represents $w_{\rm endo}$ and $w_{\rm exo}$ for $\varsigma_0 = 0$. For sufficiently low gluing numbers $w_{\rm circ}$ is the energy minimum. As η exceeds the critical value $\eta^+_{\rm act}$ ($\eta^-_{\rm act}$, respectively) given by (42) partial endocytosis (exocytosis, respectively) becomes energetically favored. At the critical value given by (44)

$$\eta^{\pm} = \sqrt{\frac{1+\mu^2-\mu}{2\mu(\mu-1)}}, \tag{45}$$

the minimum is attained by complete exocytosis or endocytosis (the solid black line) with equal energy at $\varsigma_0 = 0$. Thus, for exocytosis, the transition from no contact to partial contact is continuous, while the transition to the complete expulsion is discontinuous. For endocytosis there is a discontinuous transition between the no-contact branch and the complete engulfment of the disk. In the terminology of statistical physics, these transitions are, respectively, first- and second-order phase transitions.

The role of the spontaneous curvature is evident from Equation (44): negative values of ς_0 promote endocytosis, since from (44), we have $\eta^+ < \eta^-$; while positive values of ς_0 favor exocytosis, $(\eta^+ < \eta^-)$. Whenever $\varsigma_0 \neq 0$ the black solid line (44) splits into two branches, one relative to exocytosis and the other to endocytosis, where the one with the lowest energy branch is determined by the sign of ς_0. Using Equations (43b) and (43c), the energy gap between these two branches is $\Delta w = w_{\rm endo} - w_{\rm exo} = 4\pi\varsigma_0$. From Equation (42), we also observe that the activation threshold does not depend on the spontaneous curvature. Therefore, by tuning ς_0 one can go from a situation with no contact to complete engulfment or budding.

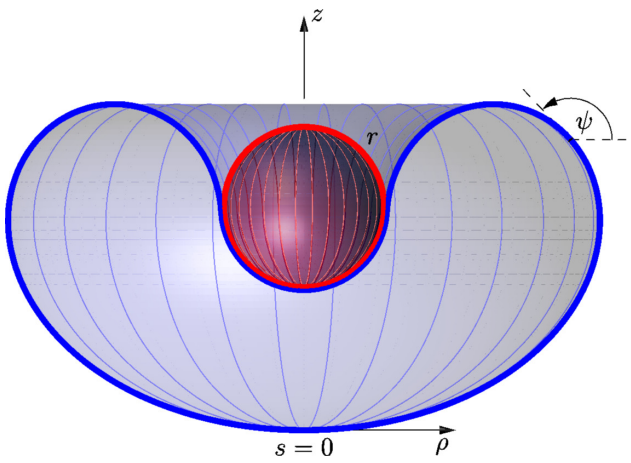

Figure 10: Schematic representation of axisymmetric partial endocytosis.

4 Adhesion of three-dimensional lipid vesicle with a rigid sphere

We turn our attention to the equilibrium shapes of a three-dimensional vesicle able to engulf or to eject a rigid spherical particle as shown in Figures 1 and 10. The volume enclosed by the vesicle may be constrained depending on the chemical properties of the system. If water is essentially free to permeate the membrane, there is no volume constraint. However, if water is unable to permeate the bilayer, the equilibrium equations have to include a fixed-volume constraint.

We consider a biological membrane with assigned unstrained area A_0, spontaneous mean curvature c_0, bending rigidity $k > 0$, and saddle-splay modulus $\bar{k}$. This membrane is put in contact with a rigid sphere of radius r and the difference of surface tension at the interface is $\Delta\gamma > 0$.

According to Helfrich's *spontaneous curvature model* [16], the bending energy of the free and contact regions are

$$W_{\rm b} = \int_{\Sigma_{\rm f}} [2k(H_{\rm f} - c_0)^2 + \bar{k}K_{\rm f}]{\rm d}a + \int_{\Sigma_{\rm c}} [2k(H_{\rm c} - c_0)^2 + \bar{k}K_{\rm c}]{\rm d}a, \tag{46}$$

where H and K denote the mean and the Gaussian curvature, respectively, while the subscripts 'f' and 'c' refers to the free and the contact regions, respectively. For instance, $\Sigma_{\rm f}$ and $\Sigma_{\rm c}$ are the free and contact interfaces, respectively.

It is important to observe that k is always positive, while various authors have reported negative values for $\bar{k}$ [37]. However, since the vesicle is closed the *Gauss-Bonnet theorem* assures that the energy term involving the Gaussian curvature is constant and, hence, does not take part in equilibrium equations as long as there is no change of topology. However, it may play a role when a change of topology occurs, which is the case for complete endocytosis and exocytosis.

Since the contact region is a portion of a spherical surface, we have

$$H_{\rm c} = \pm\frac{-1}{r}, \qquad K_{\rm c} = \frac{1}{r^2}, \qquad ((+)\text{ endocytosis, (-) exocytosis}). \tag{47}$$

We restrict our attention to axisymmetric shapes and parametrize $\Sigma_{\rm f}$ with the cylindrical coordinates

$\rho(s)$ and $z(s)$, such that $\mathbf{p}-\mathbf{0}=\rho\mathbf{e}_r+z\mathbf{e}_z$ (Figure 10). Consequently, we have

$$H_{\mathrm{f}}=\frac{1}{2}\left(\frac{\sin\psi}{\rho}+\psi'\right),\qquad K_{\mathrm{f}}=\frac{\psi'\sin\psi}{\rho}, \tag{48}$$

where $\psi(s)$ denotes the angle between the tangent to the generating curve and the plane orthogonal to the symmetry axis (see Sec. 4.6 of [38]). Once the value of $\psi(s)$ is known, the shape is given by integrating

$$\rho'=\cos\psi,\qquad z'=\sin\psi. \tag{49}$$

For definition, we set the origin so that the free region is in the interval $s\in[0,\bar{s}]$, while the contact region corresponds to value of $s\in[\bar{s},\ell]$. Unlike the planar case, where the total length is known, in the three-dimensional case both $\bar{s}$ and ℓ are unknown a priori. The generating curve for the contact region is an arc of circumference of radius r, hence we have

$$\rho(s)=r\sin\theta,\quad z(s)=z_0\pm(-r\cos\theta),\quad \psi'=\pm\frac{-1}{r},\quad ((+)\text{ endocytosis, (-) exocytosis}) \tag{50}$$

where z_0 is the z-coordinate of the rigid sphere center and $\theta=(\ell-s)/r\in[0,\bar{\theta}]$, where $\bar{\theta}$ represents, as before, the wrapping angle

$$\bar{\theta}:=\frac{\ell-\bar{s}}{r}. \tag{51}$$

By replacing (47), (48) and (50) into (46), we obtain

$$W_{\mathrm{b}}=4\pi k\int_0^{\bar{s}}\left[\frac{1}{2}\left(\frac{\sin\psi}{\rho}+\psi'\right)-c_0\right]^2\rho\mathrm{d}s+4\pi r^2k\left(\pm\frac{1}{r}-c_0\right)^2(1-\cos\bar{\theta}), \tag{52}$$

while the *adhesion energy* is assumed to be proportional to the contact area

$$W_{\mathrm{c}}=-\mathrm{Area}(\Sigma_{\mathrm{c}})\Delta\gamma=-2\pi r^2(1-\cos\bar{\theta})\Delta\gamma. \tag{53}$$

The total area of the membrane A_0 and (possibly) the enclosed volume V_0 are prescribed, thus the following constraints must hold

$$A_0=\mathrm{Area}(\Sigma_{\mathrm{f}})+\mathrm{Area}(\Sigma_{\mathrm{c}})=2\pi\int_0^{\bar{s}}\rho(s)\mathrm{d}s+2\pi r^2(1-\cos\bar{\theta}), \tag{54a}$$

$$V_0=\mathrm{Vol}(\Sigma_{\mathrm{f}})\pm\mathrm{Vol}(\Sigma_{\mathrm{c}})=\pi\int_0^{\bar{s}}\rho^2\sin\psi\,\mathrm{d}s\pm\frac{4}{3}\pi r^3(2+\cos\bar{\theta})\sin^4\frac{\bar{\theta}}{2}. \tag{54b}$$

In Equation (54b), V_0 denotes the volume of the membrane enclosed liquid added to the volume of rigid particle in endocytosis, while it denotes the volume of the liquid only in endocytosis. The plus/minus refers to endocytosis/exocytosis, respectively.

The effective energy must include further terms with their Lagrange multipliers, besides W_{b} and W_{c}, whenever the constraints (49) and (54) are imposed.

4.1 Equilibrium equations

For the derivation of equilibrium equations, it is useful to split the total energy W into two terms: $W = W_\mathrm{f} + W_\mathrm{c}$. The first term W_f denotes the energy of the free (non-contact) membrane

$$W_\mathrm{f} = \int_0^{\bar{s}} w_\mathrm{f}\,\mathrm{d}s, \tag{55}$$

where

$$\frac{w_\mathrm{f}}{2\pi} = 2k\rho\left[\frac{1}{2}\left(\frac{\sin\psi}{\rho} + \psi'\right) - c_0\right]^2 + \rho\lambda - \frac{p}{2}\rho^2\sin\psi + \lambda_1(\rho' - \cos\psi) + \lambda_2(z' - \sin\psi). \tag{56}$$

Here λ and p are constant Lagrange multipliers related to the global constraints (54), while $\lambda_1(s)$ and $\lambda_2(s)$ are related to the local constraints (49). The term W_c is the energy of the contact region

$$\frac{W_\mathrm{c}}{2\pi} = \left[2k\left(\frac{1}{r} + c_0\right)^2 + \lambda - \Delta\gamma\right] r^2(1 - \cos\bar{\theta}) + \frac{2}{3}pr^3(2 + \cos\bar{\theta})\sin^4\frac{\bar{\theta}}{2}. \tag{57}$$

The Euler-Lagrange equations derived from (55), valid for $s \in [0, \bar{s}]$, are

$$\psi'' = \frac{\cos\psi}{\rho}\left(\frac{\sin\psi}{\rho} - \psi'\right) + \frac{\lambda_1}{k\rho}\sin\psi + \frac{p}{2k}\rho\cos\psi, \tag{58a}$$

$$\lambda_1' = \frac{k}{2}\left[(\psi'^2 - 2c_0)^2 - \frac{\sin^2\psi}{\rho^2}\right] + \lambda - p\rho\sin\psi, \tag{58b}$$

$$\lambda_2' = 0. \tag{58c}$$

These equations are coupled to Equations (49) and (54).

4.1.1 Boundary conditions

At $s = 0$, the following Dirichlet boundary conditions hold:

$$\rho(0) = 0, \qquad z(0) = 0, \qquad \psi(0) = 0. \tag{59}$$

At the contact point $s = \bar{s}$, we have

$$\rho(\bar{s}) = r\sin\bar{\theta}, \qquad \psi(\bar{s}) = \pi \pm \bar{\theta} \qquad ((+)\text{ endocytosis, (-) exocytosis}). \tag{60}$$

The arbitrariness of $z(s)$ variation at $s = \bar{s}$ gives

$$\left.\frac{\partial w_\mathrm{f}}{\partial z'}\right|_{s=\bar{s}} = 0 \quad \Leftrightarrow \quad \lambda_2(\bar{s}) = 0, \tag{61}$$

which, together with (58c), implies $\lambda_2(s) = 0$.

Following [32, Section 14], the *transversality condition* is given by

$$(\mathcal{H}_{\mathrm{c}} - \mathcal{H}_{\mathrm{f}})_{s=\bar{s}} = 0, \tag{62}$$

where

$$\mathcal{H}_{\mathrm{f}} = -w_{\mathrm{f}} + \frac{\partial w_{\mathrm{f}}}{\partial \rho'}(\rho' + \cos\bar{\theta}) + \frac{\partial w_{\mathrm{f}}}{\partial \psi'}\left(\psi' + \frac{1}{r}\right), \qquad \mathcal{H}_{\mathrm{c}} = -\frac{1}{r}\frac{\partial W_{\mathrm{c}}}{\partial \bar{\theta}}. \tag{63}$$

Thus, we recover the adhesion condition (29). This condition generalizes that of Seifert and Lipowsky [39] for adhesion on curved surfaces. A similar result has been obtained by Rosso and Virga [40] for lipid tubules.

Unlike the case of the Euler elastica treated in Section 3, the total length of the generating curve is unknown. Indeed, the same membrane area can be achieved by using curves of different lengths. In order to determine the total length, a further boundary condition is required [16]:

$$-w_{\mathrm{f}} + \frac{\partial w_{\mathrm{f}}}{\partial z'}z' + \frac{\partial w_{\mathrm{f}}}{\partial \rho'}\rho' + \frac{\partial w_{\mathrm{f}}}{\partial \psi'}\psi'\bigg|_{s=0} = 0, \tag{64}$$

that leads to

$$\lambda_1 - \frac{k}{2}\frac{\sin^2\psi}{\rho}\bigg|_{s=0} = 0. \tag{65}$$

The boundary conditions (62) and (64) arise from the fact that we are dealing with a variation problem with non-fixed ends leading to transversality conditions.

4.2 Analysis

We introduce $R = \sqrt{A_0/4\pi}$ and define μ and η as in the previous Section. We also introduce the dimensionless spontaneous curvature $\sigma_0 := c_0 R$, where c_0 is the spontaneous mean curvature, saddle-splay modulus $\kappa := \bar{k}/k$ and reduced energy $w := W/k$. To treat the fixed-volume case, we introduce the reduced volume

$$\upsilon := \frac{3V_0}{4\pi R^3}. \tag{66}$$

4.2.1 Permeable vesicles

We first consider completely permeable vesicles for which the enclosed volume is not constrained. Figure 11 shows examples of equilibrium shapes for partial endocytosis and exocytosis for different wrapping angles. A substantial difference with the planar case emerges and can be appreciated by comparing Figure 11 with Figures 6 and 7. The elastica bending energy penalizes the Frenet curvature, preventing the formation of narrow necks that require a large curvature. As a consequence, the membrane globally deforms in order to accommodate the boundary conditions at the contact point, favoring the smoothness of the profile. In contrast, for a Helfrich membrane, a narrow neck has a low energetic cost. Indeed, three-dimensional necks are hyperbolic surfaces where the large main curvature along the profile can be compensated by the main curvature (of opposite sign) along

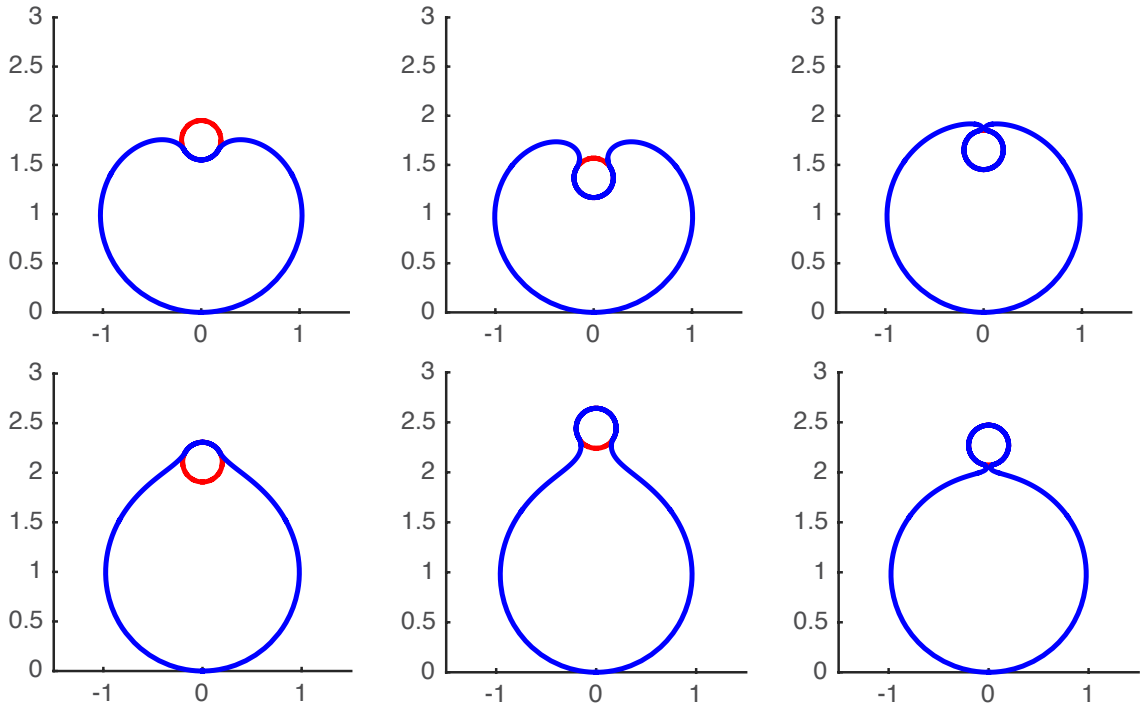

Figure 11: Equilibrium shapes for partial endocytosis (top) and exocytosis (bottom) for completely permeable vesicles ($\mu = 5$, $\sigma_0 = 0$). From left to right $\bar{\theta} = 60°, 120°, 164°$. For endocytosis $\eta = 1.62, 1.15, 1.71$, while for exocytosis $\eta = 1.29, 1.52, 2.00$.

the parallels, leading to very small mean curvatures. Therefore, highly localized deformations with low energetic costs are allowed and preferred.

For a vesicle area A_0 and in the absence of external forces, a sphere of radius R is an equilibrium shape, with reduced energy

$$w_{\text{sph}} = 4\pi[2\,(1-\sigma_0)^2 + \kappa]. \tag{67}$$

The energy corresponding to complete endocytosis is given by the energy of a spherical vesicle of area $A_{\text{f}} = 4\pi(R^2 - r^2)$, added to the energy of the endosome of area $A_{\text{e}} = 4\pi r^2$:

$$w_{\text{endo}} = 8\pi\mu^{-1}\left[-2(\sqrt{\mu^2-1}-1)\sigma_0 + \mu(2+\sigma_0)^2\right] + 4\pi(-\eta^2 + 2\kappa). \tag{68}$$

Observe that the dependance of w_{endo} on the saddle-splay modulus is $8\pi\kappa$ whereas it is $4\pi\kappa$ in w_{sph}. This difference is easily explained by applying the Gauss-Bonnet theorem and by the obvious fact that two separate spheres have a Euler-Poincaré characteristic twice that of a single sphere. Hence, during a change of topology corresponding to complete endocytosis, this part of the energy

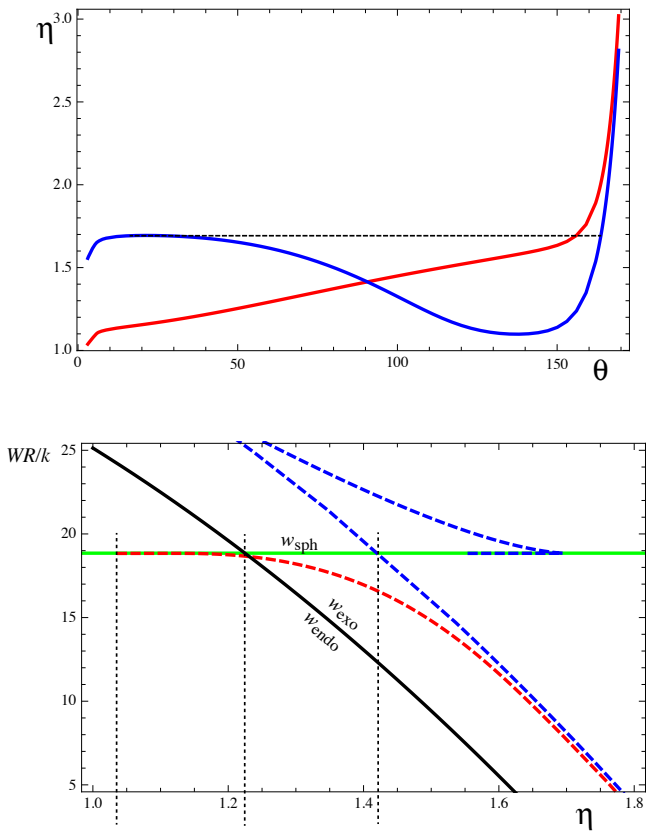

Figure 12: Permeable vesicles ($\mu = 5$, $\sigma_0 = 0$, $\kappa = -1/2$). (Top) Gluing number as a function of the wrapping angle. For exocytosis (red) the angle is strictly increasing with the gluing number, while for exocytosis (blue) it is not monotonic. (Bottom) Energy landscape: reduced energy versus gluing number. The green line is w_{sph}. The solid black line represents the reduced energy for complete endocytosis and exocytosis. The red and blue dashed curves refer to partial exocytosis and endocytosis, respectively.

is reduced by this topological change whenever κ is negative. A similar formula holds for the case of complete exocytosis:

$$w_{\text{exo}} = 8\pi\mu^{-1}\left[-2(\sqrt{\mu^2-1}+1)\sigma_0 + \mu(2+\sigma_0)^2\right] + 4\pi(-\eta^2+2\kappa). \tag{69}$$

In the following, the reduced energy relative to partial endocytosis and exocytosis is computed by numerically solving the equilibrium equations.

Direct inspection of Equations (67), (68), and (69) reveals that the spontaneous curvature σ_0 plays a role in the energy landscape, and that if κ is negative, the contribution of the saddle-splay energy promotes the fission of the membrane.

In Figure 12 we show the wrapping angle $\bar{\theta}$ as a function of the gluing number η and the energy landscape for $\mu = 5$ and $\sigma_0 = 0$. The graphs $\eta(\bar{\theta})$ show that as a consequence of a continuous binding a continuum (discontinuous) engulfment transition in exocytosis (endocytosis) occurs. Furthermore, numerical simulations show that the gluing number diverges as the wrapping angle approaches total

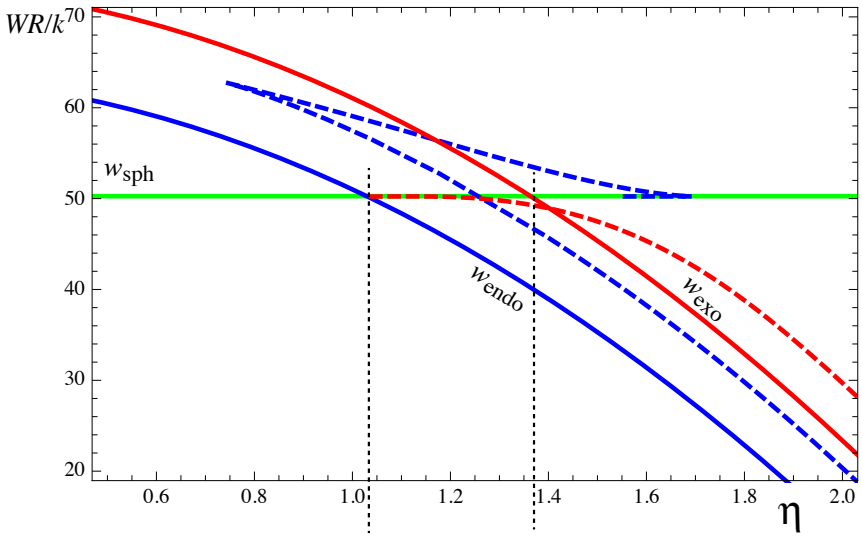

Figure 13: Permeable vesicles ($\mu = 5$, $\sigma_0 = -1/2$ and $\kappa = -1/2$). Energy landscape, reduced energy versus gluing number. The green line represents $w_{\rm sph}$. The solid blue line represents $w_{\rm endo}$. The red and blue dashed lines refer to the partial exocytosis and endocytosis, respectively.

engulfment. Accordingly, the adhesion energy becomes the dominant term and tends to minus infinity. As η tends to infinity the energetic cost of the connecting neck can be neglected and the energy tends to $w_{\rm endo} - 4\pi\kappa$ for endocytosis and $w_{\rm exo} - 4\pi\kappa$ for exocytosis (for $\sigma_0 = 0$, these energies coincide). The black solid line in Figure 12 (bottom) represents $w_{\rm endo} = w_{\rm exo}$ (since $\sigma_0 = 0$).

In summary, from the energy landscape, we deduce that for low values of η no interaction takes place. As η exceeds about 1, partial exocytosis is the minimum energy configuration. At a critical value of η (given by the intersection between the dashed red and solid black line), complete exocytosis takes place as a discontinuous transition. Complete endocytosis takes place directly at a critical value $\eta_{\rm endo} = \sqrt{2+\kappa}$, given by equating (67) and (68).

An important result of this analysis is that the topological transition, *i.e.* the complete engulfment or ejection, is driven by the saddle-splay modulus κ. Indeed, whenever $\kappa = 0$, fission is never energetically favored and budding should not take place without other active mechanisms.

The energy landscape is also affected by spontaneous curvature. As an example, consider the case $\sigma_0 = -1/2$ (Figure 13). Unlike the previous case, the branches corresponding to complete exocytosis and endocytosis have different energies. In particular, endocytosis occurs at a gluing number lower than the one found for exocytosis. Endocytosis occurs discontinuously from the no-contact branch. However, as κ approaches zero, the continuous blue curve moves upwards and the scenario changes: first, there is a continuous transition from non-interacting configuration to partial endocytosis and then a discontinuous transition to complete endocytosis.

4.2.2 Impermeable vesicles

Helfrich's model with constrained volume admits a wide variety of equilibrium shapes. When $\sigma_0 = 0$ prolate-shaped vesicles are stable for $0.65 \lesssim \upsilon < 1$, while stomatocyte shapes become the lower energy branch for $\upsilon \lesssim 0.59$. For $0.59 \lesssim \upsilon \lesssim 0.65$, oblate-discocyte shapes become energetically

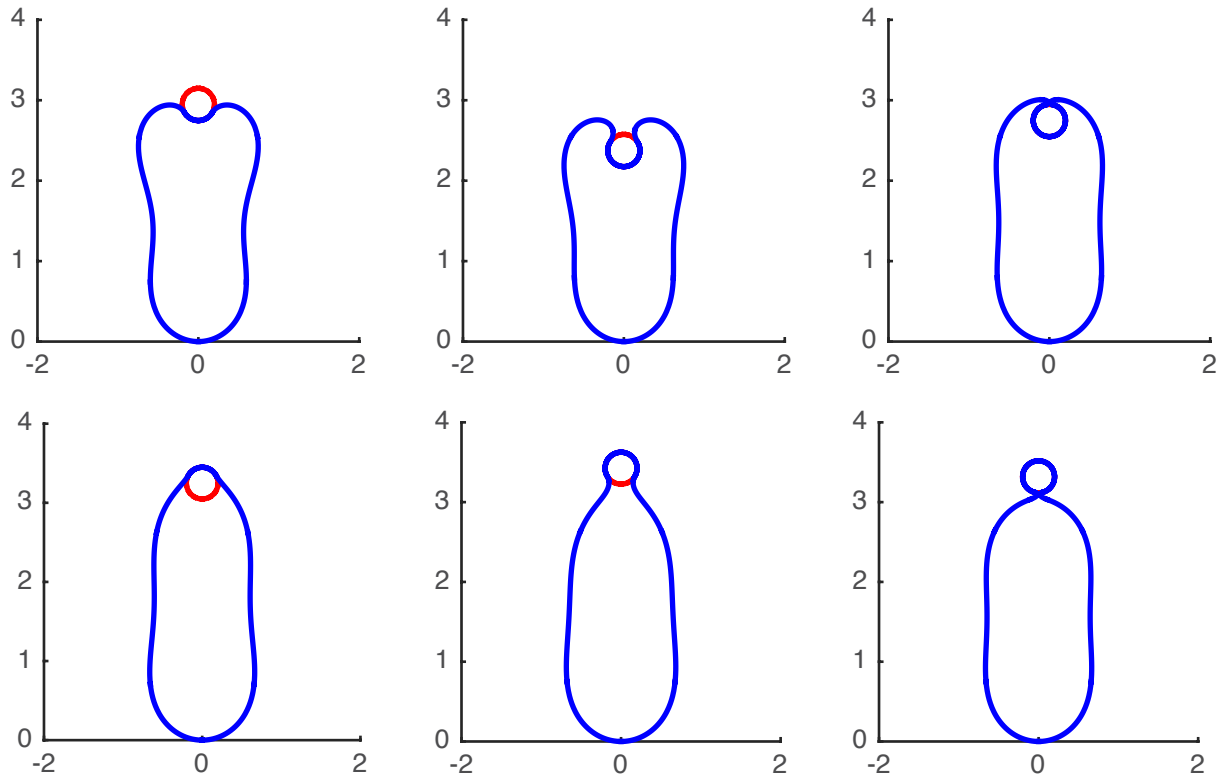

Figure 14: Equilibrium shapes for partial endocytosis (top) and exocytosis (bottom) for prolate-shaped vesicles ($\mu = 5$, $\sigma_0 = 0$, $\upsilon = 0.80$). From left to right $\bar{\theta} = 60°, 120°, 164°$. For endocytosis $\eta = 1.60, 0.95, 1.69$, while for exocytosis $\eta = 1.10, 1.53, 2.15$

favored.

Strictly speaking, the comparison between endocytosis and exocytosis should be made with the same enclosed liquid volume. Thus, by denoting υ to be the reduced volume of the liquid, and $\Delta\upsilon = \mu^{-3}$ the reduced volume of the rigid particle, the initial reduced volume for endocytosis is $\upsilon^{(\mathrm{i})}_{\mathrm{endo}} = \upsilon$, while for exocytosis it is $\upsilon^{(\mathrm{i})}_{\mathrm{exo}} = \upsilon + \Delta\upsilon$. The initial reduced membrane area is assumed to be $a^{(\mathrm{i})} = 4\pi$. As the engulfment is completed the reduced volume becomes $\upsilon^{(\mathrm{f})}_{\mathrm{endo}} = \upsilon + \Delta\upsilon$, while the area of the free membrane become $a^{(\mathrm{f})} = a^{(\mathrm{i})} - \Delta a$, where $\Delta a = 4\pi/\mu^2$ is the reduced area of the rigid particle. For complete exocytosis $\upsilon^{(\mathrm{f})}_{\mathrm{endo}} = \upsilon$.

Figure 14 illustrates partial endocytosis and exocytosis for prolate-shaped vesicles with a reduced volume $\upsilon = 0.8$, for particular values of the wrapping angle $\bar{\theta}$. When the engulfment is almost complete (right top and bottom Figure 14), the narrow neck has a negligible energetic cost. Then, the shape of the non-contact membrane tends to a prolate vesicle of enclosed reduced volume $\upsilon^{(f)}_{\mathrm{endo}}$ (for endocytosis) or $\upsilon^{(f)}_{\mathrm{exo}}$ (for exocytosis) and reduced area $a^{(f)}$. However, since that the rigid particle is small, the elastic energy of the non-contact region of the membrane does not differ much from that of the initial vesicle. The major contribution to the energy difference is due to the contact

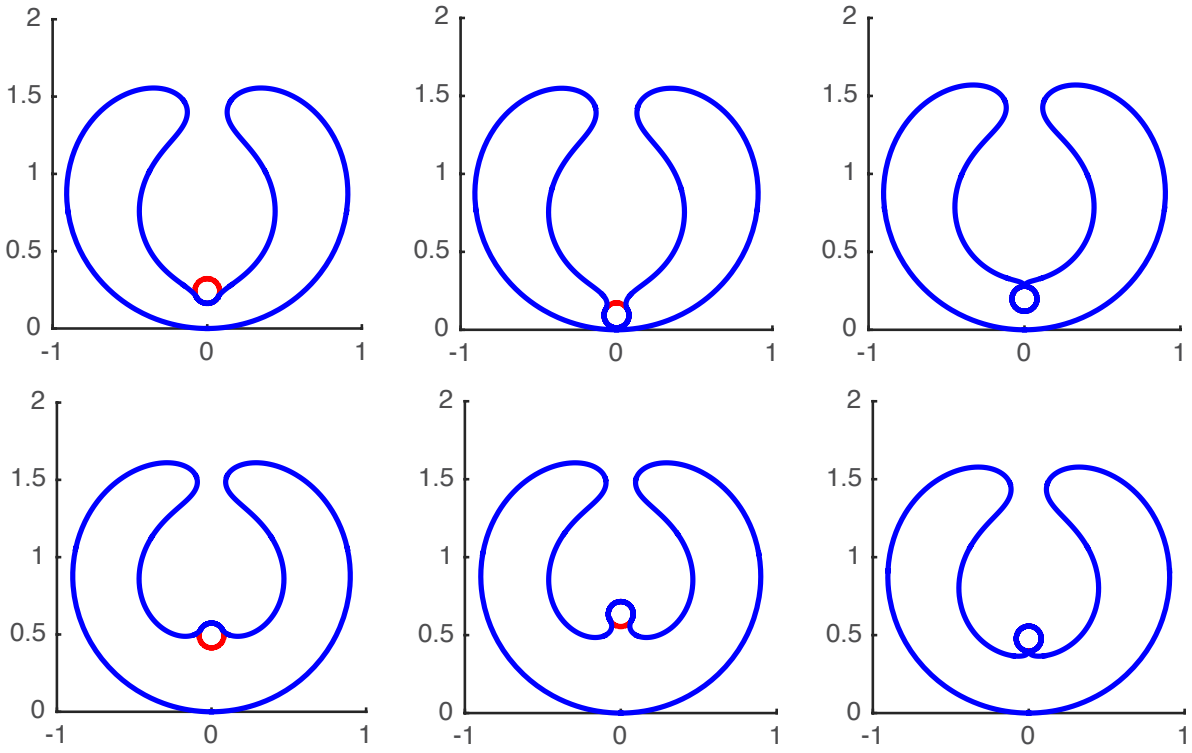

Figure 15: Equilibrium shapes for partial endocytosis (top) and exocytosis (bottom) for stomatocyte-shaped vesicles ($\mu = 12.5$, $\sigma_0 = 0$, $\upsilon = 0.58$). From left to right $\bar{\theta} = 60°, 120°, 164°$. For endocytosis $\eta = 1.30, 1.51, 3.03$, while for exocytosis $\eta = 1.58, 1.20, 2.47$.

part. The energy landscape (not shown) exhibits the same qualitative behavior as for the case of a permeable vesicle.

The energetic behavior drastically changes in stomatocyte-shaped vesicles, where the particle adheres to a region with negative mean curvature (Figure 15). In contrast to the previous cases, partial endocytosis is now a continuous process as η increases, while exocytosis is discontinuous (Figure 16 top). In the energy landscape (Figure 16 bottom) partial endocytosis is energetically favored compared to exocytosis. The black line, representing both complete endocytosis and exocytosis, splits under a change of the saddle-splay modulus.

5 Conclusions

Elastocytosis is the general process of wrapping a rigid particle by a deformed elastic structure. Here, we have studied three different instances of this phenomenon when the deformable body is a liquid droplet, an elastic ring, or a lipid vesicle. The physical tendency to wrap is encoded in the gluing number: the ratio of the disk radius by the elasto-capillary length. We have analyzed shape transformations as a function of the gluing number and have illustrated the energy landscape

related to different solution branches. The following general observations emerge from our analysis.

Liquid droplet: This model allows us to mimic the processes of endocytosis and exocytosis. The process of engulfment or ejection takes place continuously, as the surface tension at the solid-liquid interface changes. The shape of the deformable body is always a sphere, whose radius is constant in an isobaric process but varies in an isochoric transformation.

Planar elastic ring: When an elastic ring interacts with an adhesive rigid disk, the equations governing the shapes are integrable. The contact interaction induces long-range distortions on the ring, and equilibrium shapes are characterized by a smooth curvature profile. This behavior is due to the contribution of the bending energy that penalizes high Frenet curvatures, thus preventing the formation of narrow necks.

It is possible to obtain analytically the critical value of the gluing number beyond which partial or complete elastocytosis takes place. It is also important to note that there is a difference between wrapping a particle which is inside and outside of the ring because the signed curvature of the ring either matches the curvature of the disk or not. However, these critical values depend only on the geometric parameter μ. The complete process, with the formation of a separate elastosome (the disk wrapped by an elastic membrane) can be solely driven by surface tension. The spontaneous curvature does not influence the equilibrium shapes but plays a role in the energy landscape and affects the threshold value at which complete elastocytosis occurs.

Lipid vesicles: When a rigid sphere adheres to an axisymmetric lipid membrane, our analysis shows that the shape is mostly deformed in the vicinity of the contact point. An important property of the Helfrich model is that it allows high curvatures when they have similar magnitude but opposite signs as they give a small mean curvature. Therefore, narrow necks can be formed at a low energetic cost. However, due to the sudden change in the curvature profile at the contact point, total wrapping (without detachment from the parent cell) can only be achieved asymptotically as it requires an infinite gluing number. From the energy landscape, it emerges that, as $\eta \to \infty$, the bending energy approaches from above the energy associated with complete separation. This property implies the existence of an energy barrier that leads us to conclude that surface tension alone is not sufficient to guarantee the detachment from the parent cell. Thus, the contribution of the Gaussian curvature energy becomes crucial in providing the energy gap needed for splitting.

As in the planar case, different behaviors are observed when wrapping a particle that is inside or outside the vesicle. Both continuous and discontinuous transitions may occur during wrapping, depending on the spontaneous curvature.

Our analysis provides a clear picture of the possible transitions that can occur when a particle is presented to a membrane. Obviously, the cellular world is infinitely more complicated, and it is well appreciated than many active processes are involved in these events. Yet, the rich structure of profiles and possible behaviors suggest that biological systems can tap into the physical properties of these membranes and achieve different functions by modifying actively internal parameters.

Acknowledgments– This work was supported by the Engineering and Physical Sciences Research Council grant EP/R020205/1 to Alain Goriely. The work of Gaetano Napoli has been funded by the MIUR (Italian Ministry of Education, University and Research) project PRIN 2017, "Mathematics

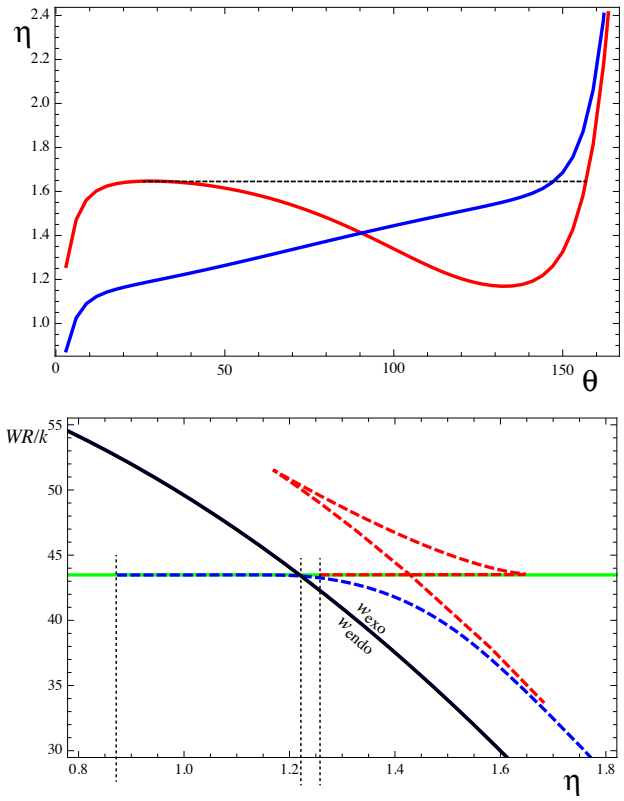

Figure 16: Prolate-shaped vesicles ($\upsilon = 0.8$, $\mu = 5$, $\sigma_0 = 0$, $\kappa = -1/2$). (Top) Gluing number as a function of the wrapping angle. For exocytosis (red) the trend is increasing, while for exocytosis (blue) it is not monotonous. (Bottom) Energy landscape, reduced energy versus gluing number. The green line represents $w_{\rm sph}$. The solid line represents the reduced energy for complete endocytosis and exocytosis. The red and blue dashed curves refer to partial exocytosis and endocytosis, respectively.

of active materials: From mechanobiology to smart devices", project n. 2017KL4EF3.

References

[1] A Michaelis, MM Green, and Rigomar Rieger. *Glossary of Genetics: Classical and Molecular*. Springer-Verlag, 1991.

[2] Maurice B Hallett and Sharon Dewitt. Ironing out the wrinkles of neutrophil phagocytosis. *Trends in cell biology*, 17(5):209–214, 2007.

[3] Alan Aderem and David M Underhill. Mechanisms of phagocytosis in macrophages. *Annual review of immunology*, 17(1):593–623, 1999.

[4] Lee-Ann H Allen and Alan Aderem. Mechanisms of phagocytosis. *Current opinion in immunology*, 8(1):36–40, 1996.

[5] James W Booth, William S Trimble, and Sergio Grinstein. Membrane dynamics in phagocytosis. In *Seminars in immunology*, volume 13, pages 357–364. Elsevier, 2001.

[6] Marc Herant, Volkmar Heinrich, and Micah Dembo. Mechanics of neutrophil phagocytosis: behavior of the cortical tension. *Journal of cell science*, 118(9):1789–1797, 2005.

[7] Marc Herant, Volkmar Heinrich, and Micah Dembo. Mechanics of neutrophil phagocytosis: experiments and quantitative models. *Journal of cell science*, 119(9):1903–1913, 2006.

[8] Reinhard Lipowsky. Response of membranes and vesicles to capillary forces arising from aqueous two-phase systems and water-in-water droplets. *The Journal of Physical Chemistry B*, 122(13):3572–3586, 2018.

[9] Yi Zhang, Abiola Shitta, J Carson Meredith, and Sven H Behrens. Bubble meets droplet: Particle-assisted reconfiguration of wetting morphologies in colloidal multiphase systems. *small*, 12(24):3309–3319, 2016.

[10] G Napoli and A Goriely. A tale of two nested elastic rings. *Proceedings of the Royal Society A: Mathematical, Physical and Engineering Sciences*, 473(2204):20170340, 2017.

[11] Jeff ZY Chen and Sergey Mkrtchyan. Adhesion between a rigid cylindrical particle and a soft fluid membrane tube. *Physical Review E*, 81(4):041906, 2010.

[12] Xin Yi and Huajian Gao. Phase diagrams and morphological evolution in wrapping of rod-shaped elastic nanoparticles by cell membrane: a two-dimensional study. *Physical Review E*, 89(6):062712, 2014.

[13] F Bosi, D Misseroni, F Dal Corso, and D Bigoni. Self-encapsulation, or the 'dripping'of an elastic rod. *Proceedings of the Royal Society A: Mathematical, Physical and Engineering Sciences*, 471(2179):20150195, 2015.

[14] J. H. Fuhrhop and W. Helfrich. Fluid and solid fibers made of lipid molecular bilayers. *Chem. Rev.*, 93:1565–1582, 1993.

[15] W. Helfrich and J. Prost. Intrinsic bending force in anisotropic membranes made of chiral molecules. *Phys. Rev. A*, 38:3065–3068, 1988.

[16] U. Seifert, K. Berndl, and R. Lipowsky. Shape transformations of vesicles: Phase diagram for spontaneous- curvature and bilayer-coupling models. *Phys. Rev. Aview A*, 44(2):1182–1202, 1991.

[17] Jean-Marc Allain and Martine Ben Amar. Biphasic vesicle: instability induced by adsorption of proteins. *Physica A: Statistical Mechanics and its Applications*, 337(3-4):531–545, 2004.

[18] J-M Allain and M Ben Amar. Budding and fission of a multiphase vesicle. *The European Physical Journal E*, 20(4):409–420, 2006.

[19] Susanne F Fenz and Kheya Sengupta. Giant vesicles as cell models. *Integrative Biology*, 4(9):982–995, 2012.

[20] Markus Deserno. When do fluid membranes engulf sticky colloids? *Journal of Physics: Condensed Matter*, 16(22):S2061, 2004.

[21] Sabyasachi Dasgupta, Thorsten Auth, and Gerhard Gompper. Wrapping of ellipsoidal nanoparticles by fluid membranes. *Soft Matter*, 9(22):5473–5482, 2013.

[22] W. T. Góźdź. Deformations of lipid vesicles induced by attached spherical particles. *Langmuir*, 23(10):5665–5669, 05 2007.

[23] Siqin Cao, Guanghong Wei, and Jeff ZY Chen. Transformation of an oblate-shaped vesicle induced by an adhering spherical particle. *Physical Review E*, 84(5):050901, 2011.

[24] Xin Yi and Huajian Gao. Incorporation of soft particles into lipid vesicles: Effects of particle size and elasticity. *Langmuir*, 32(49):13252–13260, 12 2016.

[25] Xin Yi and Huajian Gao. Budding of an adhesive elastic particle out of a lipid vesicle. *ACS Biomaterials Science & Engineering*, 3(11):2954–2961, 11 2017.

[26] Jee E Rim, Prashant K Purohit, and William S Klug. Mechanical collapse of confined fluid membrane vesicles. *Biomech. Model. Mechan.*, 13(6):1277–1288, 2014.

[27] O. Kahraman, N. Stoop, and M. M. Müller. Morphogenesis of membrane invaginations in spherical confinement. *EPL*, 97(6):68008, 2012.

[28] Jaime Agudo-Canalejo and Reinhard Lipowsky. Critical particle sizes for the engulfment of nanoparticles by membranes and vesicles with bilayer asymmetry. *ACS Nano*, 9(4):3704–3720, 04 2015.

[29] Amir Houshang Bahrami, Reinhard Lipowsky, and Thomas R. Weikl. The role of membrane curvature for the wrapping of nanoparticles. *Soft Matter*, 12(2):581–587, 2016.

[30] P. G. De Gennes, F. Brochard-Wyart, and D. Quéré. *Capillarity and wetting phenomena: drops, bubbles, pearls, waves*. Springer Verlag, 2004.

[31] A. Goriely. *The Mathematics and Mechanics of Biological Growth*. Springer Verlag, New York, 2017.

[32] I. M. Gelfand and S. V. Fomin. *Calculus of variations*. Prentice Hall, 1963.

[33] R. De Pascalis, G. Napoli, and S , Turzi. Growth-induced blisters in a circular tube. *Physica D*, 283:1–9, 2014.

[34] D. Vella, J. Bico, A. Boudaoud, B. Roman, and P. M. Reis. The macroscopic delamination of thin films from elastic substrates. *Proc. Natl. Acad. Sci. USA*, 106(27):10901–10906, 2009.

[35] A. Goriely and M. Nizette. Kovalevskaya rods and Kovalevskaya waves. *Regul. Chaotic Dyn.*, 5:95–106, 2000.

[36] M. Abramowitz and I. A. Stegun. *Handbook of Mathematical Function with Formulas, Graphs, and Mathematical Tables*. Dover, New York, 1964.

[37] Brian Seguin and Eliot Fried. Calculating the bending moduli of the canham–helfrich free-energy density. In Gui-Qiang G. Chen, Michael Grinfeld, and R. J. Knops, editors, *Differential Geometry and Continuum Mechanics*, pages 345–361, Cham, 2015. Springer International Publishing.

[38] Z-C Ou-Yang, J-X Liu, and Y-Z Xie. *Geometric methods in the elastic theory of membranes in liquid crystal phases*. Number 2 in Advanced Series on Theoretical Physical Science. World Scientific. Singapore, 1999.

[39] U. Seifert and R. Lipowsky. Adhesion of vesicles. *Phys. Rev. A*, 42(8):4768–4771, 1990.

[40] R Rosso and E. G. Virga. Adhesion by curvature of lipid tubules. *Continuum. Mech. Thermodyn.*, 10(6):359–367, 1998.